ELSEVIER

Dynamics of Atmospheres and Oceans 24 (1996) 183–195

dynamics of atmospheres and oceans

Mixing in lock-release gravity currents

J. Hacker *, P.F. Linden, S.B. Dalziel

Department of Applied Mathematics and Theoretical Physics, Silver Street, Cambridge CB3 9EW, UK

Received 1 July 1994; revised 3 February 1995; accepted 24 February 1995

Abstract

The density front bounding a gravity current is usually highly unstable and this leads to mixing between the fluid of the gravity current and that of the surroundings. This mixing plays an important part in the dynamics of gravity currents and determines how fluid properties are transported and distributed by the flow. In this paper we describe a new experimental technique to determine the density structure of gravity currents, and present some results for the lock-release case. We find that substantial mixing occurs in the early stages of the evolution of lock-release gravity currents and that this mixing leads to the formation of a complex internal density structure. Mixed fluid is produced across the concentration range and we examine the mixing rates. By contrasting three experiments with different lock aspect ratios, we examine the effect of the aspect ratio of the release on the subsequent evolution of the flow.

1. Introduction

Gravity currents are produced when fluid of one density is released into fluid of a different density at a horizontal boundary. The variation in buoyancy force along the boundary, which is caused by the density difference, produces a horizontal pressure gradient which drives a flow along the boundary. Typically, this flow has the form of a penetrating current bounded downstream by a strong frontal region, called the 'head', and a shallower following flow, called the 'tail' (Simpson, 1987).

The simplest situation, and the one we shall consider in this paper, is the lock-release case. This consists of two fluids of different densities contained in a rectangular channel, initially at rest and separated by a vertical barrier. When the

* Corresponding author.

SSDI 0377-0265(95)00443-2

barrier is withdrawn the dense fluid flows along the floor of the channel underneath the less dense fluid, forming a gravity current. The lock-release flow is interesting because it exhibits dynamics which are common to a range of more complex gravity currents. Examples of these flows are accidental releases of liquefied dense gases, sea breezes and turbitity currents in the oceans. Another interesting aspect of the lock-release flow is the range of behaviour displayed by the gravity current as it evolves. This evolution has been found to occur over three distinct phases (see Simpson, 1987). In the first stage, the 'slumping phase', the head of the current travels at constant speed and maintains nearly constant depth. In the second stage, the 'similarity phase', the current decelerates, as $t^{-1/3}$, and decreases in depth. The transition between these two stages has been found to occur after the current has propagated approximately ten lock lengths. If the Reynolds number of the gravity current drops sufficiently, a third phase occurs in which viscous forces are important.

In most situations the head of a gravity current is highly unstable, and this leads to mixing between the fluid of the current and that of the ambient layer. There are two dominant modes of instability governing the mixing processes. The first is Kelvin–Helmholtz instability, which results in finite-amplitude billows forming at the apex of the head. The second mode of instability, which occurs only when the current is propagating along a no-slip boundary, is a convective instability known as 'lobes and clefts' (Simpson, 1972). This instability results in clefts at the base of the head which engulf ambient fluid and disrupt the span-wise symmetry of the Kelvin–Helmholtz billows.

Simpson and Britter (1979) examined these instabilities and quantified the bulk mixing rates for steady-state currents, but were not able to determine the details of the density structure produced. Recently, Hallworth et al. (1993) made use of an acid–base flow visualisation technique to investigate the lock-release case. They found that no mixing takes place during the slumping phase and that all dilution takes place during the similarity phase, with the head of the current remaining homogeneously mixed at all stages. The details of the global density structure, and the concentration distribution of the mixed fluid produced, have not been reported. This information, however, is of central importance in many situations. For example, in the case of the accidental release of a flammable gas it is desirable to determine the stage at which mixing has diluted the gas to a concentration below the flammable threshold. Other examples occur in meteorology and oceanography where it may be desirable to know how a gravity current distributes heat, salt or pollution. In addition to these practical issues, information about the internal structure of gravity currents is required if we are to understand how mixing affects the evolution of the flow.

In this paper we describe a new experimental technique to determine the internal density structure of lock-release gravity currents flowing in a rectangular channel. From the results we examine the evolution of the internal structure and investigate the quantity and concentrations of mixed fluid produced. In particular, we examine the effects of changes in the aspect ratio of the lock. In Section 2 the experiments and the measurement technique are described. In Section 3 the

results are presented and discussed. In Section 4 the results are summarised and the conclusions given.

2. The experiments

The experiment were carried out in a rectangular Perspex channel of 205 mm width, 500 mm depth and 3480 mm length. On one side of the channel four fluorescent strip lights were positioned behind a light-diffusing screen to provide nearly uniform back-lighting.

Each experiment was performed as follows. The channel was filled with water to a depth H. A vertical gate was then positioned at a distance x_0 from one end of the channel to form a lock. A quantity of salt was dissolved into the water of the lock to create a density difference $\Delta\rho$. In all of the experiments reported here $\Delta\rho$ was such that the reduced gravity $g' \equiv (\Delta\rho/\rho_0)$ was 120 mm s^{-2}, where ρ_0 is the density of the ambient fluid. A measured quantity of dye was also added to the water in the lock to provide flow visualisation. To initiate the experiment the gate was smoothly withdrawn, leaving the dense fluid to flow out along the floor of the channel. The progress of each experiment was recorded on videotape. For practical reasons, the video camera was kept at a fixed position and the field of view was the first half of the channel.

Three experiments are reported here. For each experiment the aspect ratio $R \equiv H/x_0$ of the lock was varied by changing the length of the lock x_0 and the total water depth H. The values taken by these parameters were: Experiment 1: $x_0 = 300$ mm, $H = 200$ mm, $R = 0.67$; Experiment 2: $x_0 = 400$ mm, $H = 400$ mm, $R = 1.00$; Experiment 3: $x_0 = 150$ mm, $H = 267$ mm, $R = 1.78$.

Measurements of density structure were made by analysing digitally the videotapes using the image processing system DigImage (Dalziel, 1993). The principle of the measurement technique is the fact that the light from the back-lighting is attenuated (absorbed) by the dye as it passes through the flow. As the gravity current mixes with the ambient fluid the dye is diluted and so less light is attenuated in regions of greater dilution. The dye may be taken to mark dense fluid and so density may be inferred from dye concentration. A similar technique was used by Holford (1994) to measure layer depth in the Rossby adjustment problem.

The measurement process involved two stages. The first stage was to measure light attenuation. If i_0 is the light intensity at a point when no dye is present, and i is the light intensity when dye is present, the attenuation is i/i_0. The image processing system digitises each frame of video by recording the light intensities at 512×512 pixel points. By dividing the intensities of pixels in an image containing dye by the intensities of the same pixels in an image taken before the introduction of the dye, i/i_0 may be determined. The values of light intensity returned by the image processing system do not correspond exactly to real-world light intensities, but the relationship was determined by calibration.

The second stage of the measurement process was to relate the mean across-

channel dye concentration to light attenuation. We assume that the light rays received by the camera passed through the channel in a direction perpendicular to the side-walls, so that the amount of dye a light ray has passed through is equal to the integral of dye concentration across the width of the channel at the location of the light ray. As the width of the channel is constant, it is permissible to divide the integrated dye concentration by the width of the channel to give the mean across-channel dye concentration C, and to relate C to i/i_0 by an expression of the form

$$C = C_0 f\left(\frac{i}{i_0}\right), \tag{1}$$

where C_0 is a reference mean concentration and f is a single-valued function, which was determined by calibration. In practice, f is a nonlinear function and care was taken to compromise between attaining a reasonable range of intensities while still working with dye concentrations within the more linear range of f.

Two checks were made to estimate the errors involved in the measurement process. The back-lighting was not completely uniform; however, (1) implies that for a given concentration of dye i/i_0 should be uniform, regardless of variations in i_0. When the channel was filled with a uniform concentration of dye, the value of i/i_0 was found to be constant to within 2% (a similar value to the noise level of the system) across most of the image, but was less satisfactory at the edges of the image, where the back-lighting was less bright. The second check made was to calculate the total amount of dye, which is constant, at successive times during each experiment. This amount was found to be constant to within 10%. This larger error is thought to be caused by errors introduced at the darker edges of the images, and by errors at higher concentration which were magnified by the nonlinearity in the dye calibration function. The necessary discretisation of the concentration field also causes cumulative errors in this quantity.

Measurements of front speed and head height were also made form the digitised images. The spatial resolution was 5 mm, and the temporal resolution was 0.04 s.

3. Results and discussion

3.1. Internal structure

Figs. 1, 2 and 3 show iso-concentration contours for Experiments 1, 2 and 3, respectively. Iso-concentration contours are plotted at values of 0.8, 0.7, 0.6, 0.5, 0.4, 0.3, 0.2, 0.1 and 0.05 of the initial concentration. Owing to the different lock lengths, Fig. 1, Fig. 2 and Fig. 3 show the evolution of the currents over propagation distances of approximately four, three and ten lock lengths, respectively.

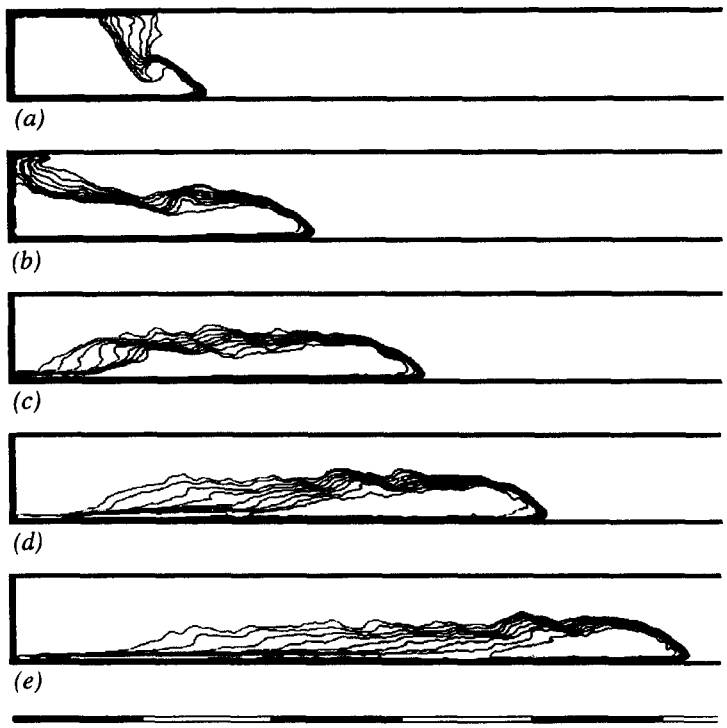

Fig. 1. Evolution of iso-concentration contours for Experiment 1, $R = 0.67$, at various values of non-dimensional front position $l = (x_f - x_0)/x_0$: (a) $l = 0.47$; (b) $l = 1.33$; (c) $l = 2.20$; (d) $l = 3.15$; (e) $l = 4.30$. The scale shown indicates lock lengths x_0.

The initial development of the flow is similar for the three cases. After the withdrawal of the gate the vertical column of dense fluid released collapses downwards to form an outflow along the base of the channel (Figs. 1(a), 2(a) and 3(a)). The collapse is initiated at the base of the column, where a characteristic gravity current head develops. Almost immediately, the head becomes unstable to the Kelvin–Helmholtz mode and rolls up to form a billow structure, which entrains ambient fluid from the rear. The billow structure is advected upwards by the following flow and a sharp leading density front is maintained. Above the head there is a more diffuse region of mixing which is caused by vortices shed from the gate during its withdrawal. The relative mixing caused by the gate is much greater for the shorter lock in Experiment 3 (Fig. 3(a)). As the current progresses Kelvin–Helmholtz waves form on the interface, and this results in further mixing, which produces stratified fluid above the interface (Figs. 1(b), 2(b) and 3(b)).

Much of this mixing is accomplished by relatively small-wavelength Kelvin–Helmholtz waves which do not preserve their structure across the width of the channel, and so cannot be identified in the mean concentration field. However, a number of coherent billow structures can be seen in Figs. 1(b), 2(b) and 3(b), which indicates that these structures are predominantly two-dimensional. In Fig. 1(b) the

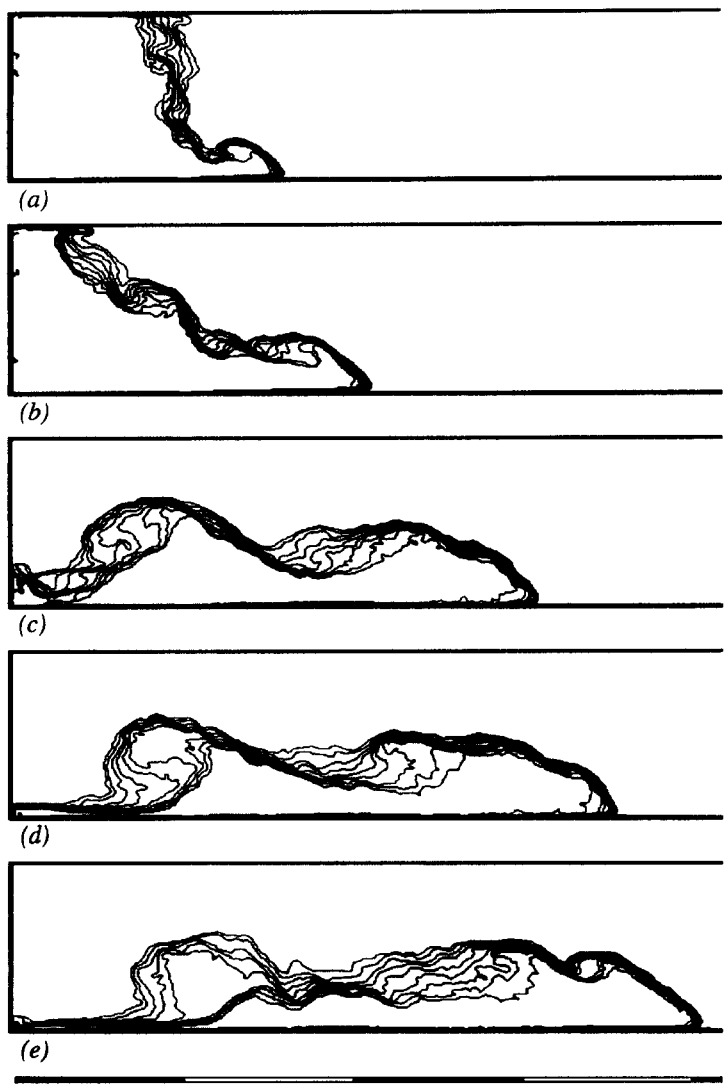

Fig. 2. Evolution of iso-concentration contours for Experiment 2, $R = 1.00$, at various values of non-dimensional front position $l = (x_f - x_0)/x_0$: (a) $l = 0.60$; (b) $l = 1.11$; (c) $l = 2.10$; (d) $l = 2.56$; (e) $l = 3.08$. The scale shown indicates lock lengths x_0.

billow which can be seen behind the head is the remnant of the initial instability of the head, seen in Fig. 1(a). In Figs. 2(b) and 3(b), however, the billows on the interface behind the head (two in Fig. 2(b), one in Fig. 3(b)) are due to Kelvin–Helmholtz instability of the sloping interface of the slumping dense fluid. These instabilities influence the subsequent development of the flow, as shall be discussed below.

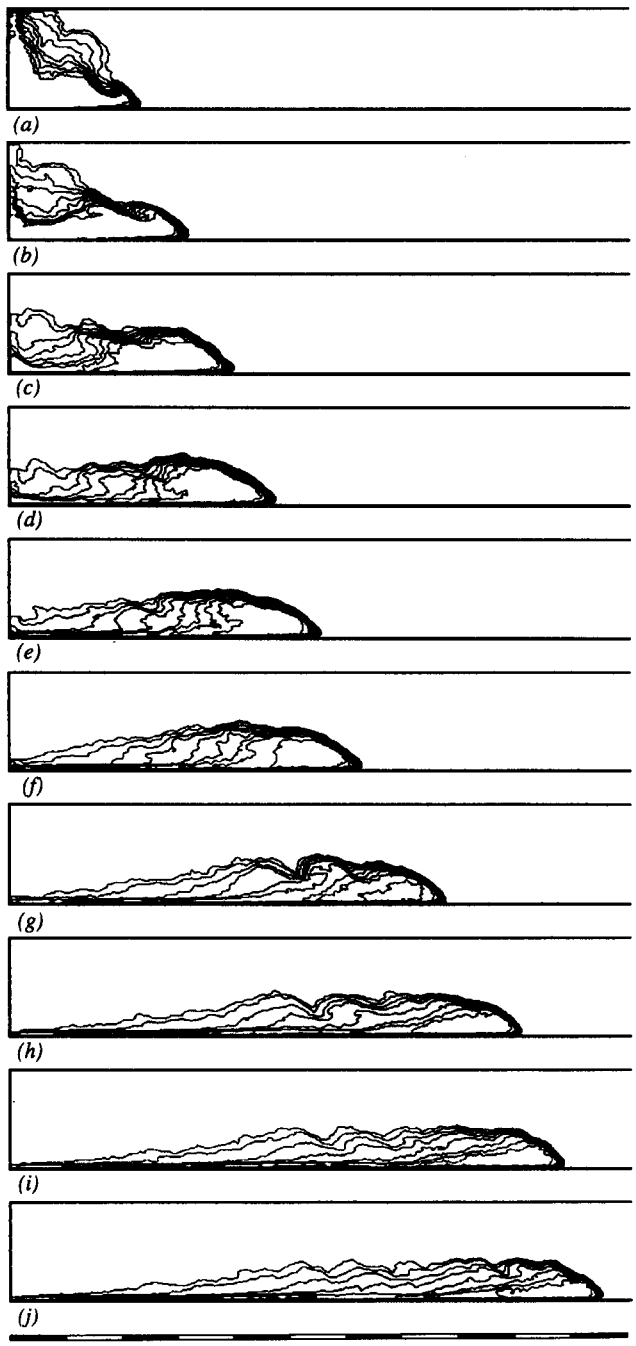

Fig. 3. Evolution of iso-concentration contours for Experiment 3, $R = 1.78$, at various values of non-dimensional front position $l = (x_f - x_0)/x_0$: (a) $l = 1.33$; (b) $l = 2.17$; (c) $l = 3.00$; (d) $l = 3.73$; (e) $l = 4.53$; (f) $l = 5.27$; (g) $l = 6.80$; (h) $l = 8.13$; (i) $l = 8.93$; (j) $l = 9.60$. The scale shown indicates lock lengths x_0.

Corresponding to the outflow of dense fluid at the base of the channel there is a flow of less dense ambient fluid above the current towards the rear wall of the channel. This counter-flowing current differs from the dense bottom current in that the density front bounding the former is much less distinct. This is probably a consequence of the asymmetry in the disturbance produced by the gate. The dense bottom current has established itself before the gate is completely withdrawn whereas the surface current has not. The surface current is also significantly disrupted by the disturbance produced as the gate passes through the free surface. Asymmetries may also be caused by the different top (free surface) and bottom (no-slip) boundary conditions, as these influence the structures of the top and bottom gravity current heads (Simpson, 1972).

By the time the current has propagated approximately one lock length, the surface current reaches the end wall of the channel (Figs. 1(b), 2(b) and 3(b)). This marks the end of the stage during which the bottom gravity current is evolving from the lock and effectively behaves as if the lock were of infinite horizontal extent. After this point in time, the surface flow ceases to be driven by a contrast in buoyancy force along the free surface, and becomes a return flow associated with the intrusion of the bottom current into the ambient layer. The return flow is reflected at the back wall to form a flow of less dense fluid behind the gravity current, and this influences the structure of the flow to the rear of the head.

The development of the flow subsequent to the reflection of the surface current is shown in parts (c)–(e) of Figs. 1–3. This development differs significantly between the three experiments.

In Experiment 1, the lower aspect ratio case of $R = 0.67$, the flow develops a classical gravity current shape with a raised head and a shallower following flow. Kelvin–Helmholtz waves continue to form at the head of the gravity current, and these break at the rear of the head, causing ambient fluid to be entrained. This mixing produces stratified fluid (Fig. 1(c)) which, as it has little forward momentum remaining, is left behind at the rear of the head and may be described as having been detrained from the head of the current. The detrained fluid is replaced by dense fluid from the rear, and the region within the head remains fairly homogeneous. As the process of detrainment continues, the region of stratification grows and the homogeneous region in the head is eroded (Figs. 1(d) and 1(e)). In Fig. 1(e) it can be seen that the region of stratification has grown to extend over almost the complete length of the current.

In Experiment 2, the case of $R = 1.00$, the structure of the flow subsequent to the reflection of surface current is very different. Here the flow at the rear of the head is dominated by a large vortex structure, which was produced by a shear instability on the interface of the slumping dense fluid (Fig. 2(b)). It is likely that the strong slope of the interface imparts a large amount of baroclinic vorticity into the vortex, and this accounts for its subsequent vigour. Dense fluid is drawn upwards into the structure, and this results in vigorous mixing (Fig. 2(c) and 2(d)). The flow of dense fluid into the vortex also impedes the flow of dense fluid into the head, and this influences the structure of the forward part of the flow. The Kelvin–Helmholtz waves which form at the head mix more deeply into the current

in this case, and produce a region of stratification between the vortex and the head (Figs. 2(c) and 2(d)). By the time the current has propagated about three lock lengths (Fig. 2(e)) the dominant rear vortex has lost most of its energy and the flow begins to bear more resemblance to that in Experiment 1.

In Experiment 3, the higher aspect ratio case of $R = 1.78$, the structure of the flow is different again. The fractional height of the head is little affected by the aspect ratio, and so in this case the high aspect ratio produces a current of length comparable with its depth. As a consequence, there is no longer a supply of dense fluid at the rear of the head, and the Kelvin–Helmholtz waves break directly into a region of mixed fluid (Figs. 3(c)–3(e)), resulting in the formation of a horizontal density structure, with near-vertical isopycnals behind the head. This horizontal density gradient is not frontogenic, as it is positive in the direction of the flow, and so becomes weaker as the current progresses, with isopycnals tilting towards the horizontal. The instability which formed on the interface of the slumping dense fluid (Fig. 3(b)) is much weaker than the corresponding vortex in Experiment 2, and influences the flow to a much lesser extent. This is, in part, a consequence of the larger influence of the disturbance caused by the withdrawal of the gate which, as can be seen by the spread of the isopycnals in Fig. 1(a), reduces the shear across the slumping interface. As the lock length is smaller in this experiment we can follow the development of the flow for a larger number of lock lengths. By the time the head of the current has travelled about five lock lengths (Fig. 3(f)) all of the fluid in the current has been mixed to some extent with the ambient fluid. The densest mixed fluid in the current is confined to the immediate region of the nose and a strong leading front is maintained. Kelvin–Helmholtz waves continue to form at the interface and these mix deeply into the current (Figs. 3(g)–3(i)) producing further stratified fluid. By the time the current has propagated ten lock lengths (Fig. 3(j)) the region of stratification extends well into the head of the current.

3.2. Entrainment rates

To quantify the mixing further, we can examine the quantity and concentrations of the mixed fluid produced. This information is shown in Fig. 4. In each of the graphs the non-dimensional volumes of fluid A/A_0, where A is volume per unit width and A_0 is the initial volume per unit width of the lock, at or above given concentration thresholds are plotted against distance propagated in terms of lock lengths. There are six sets of points in each graph which correspond to six concentration thresholds of 1.00, 0.80, 0.60, 0.40, 0.20 and 0.05 of the initial concentration. We shall refer to a set of points representing a concentration threshold as an isopleth.

The 0.05 iso-concentration contour, shown in Figs. 1–3, may be taken nominally to define the boundary of the current. The ordinate values of the 0.05 isopleth therefore correspond to the total volume of the current, and the slope of the 0.05 isopleth corresponds to the total rate of entrainment of ambient fluid. In all three cases (Figs. 4(a)–4(c)) the slopes of the 0.05 isopleths, after the initial rapid

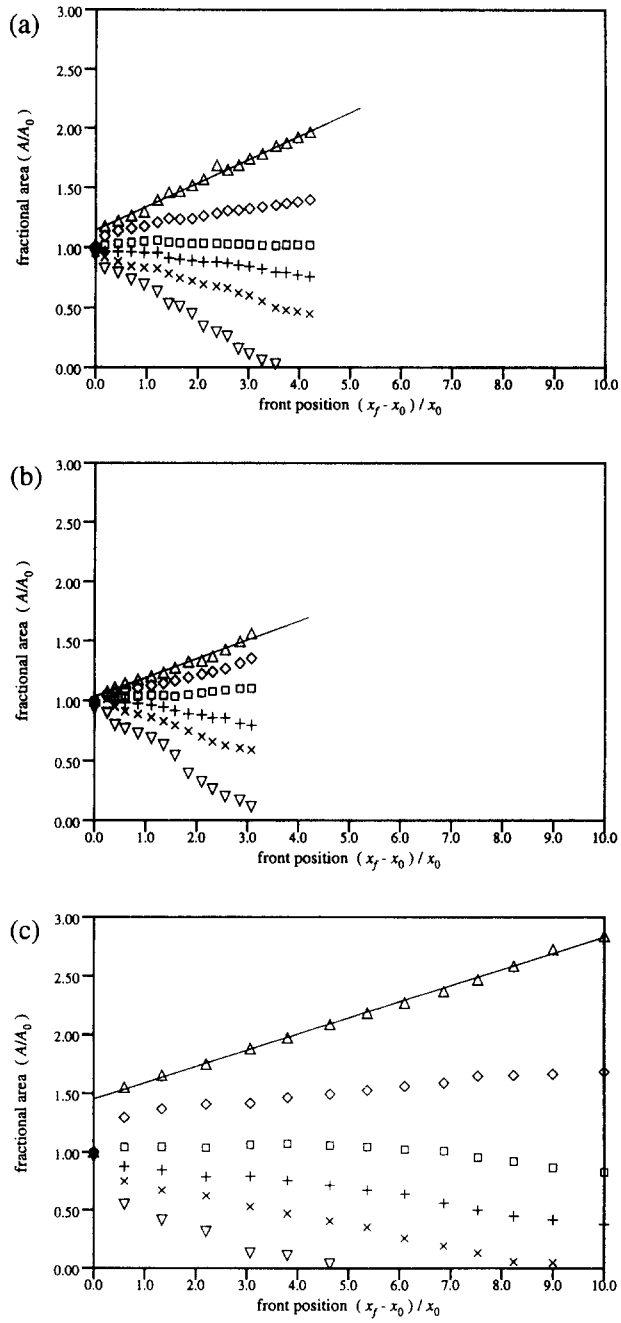

Fig. 4. Fractional areas A/A_0 below given concentration thresholds as a function of non-dimensional front position $l=(x_f-x_0)/x_0$ for: (a) Experiment 1, $R=0.67$; (b) Experiment 2, $R=1.00$; (b) Experiment 3, $R=1.78$. Isopleths are denoted for various nondimensional concentration thresholds: △: 0.05; ◇: 0.20; □: 0.40; +: 0.60; ×: 0.80; ▽: 1.00.

entrainment owing to the withdrawal of the gate, are approximately constant. This indicates that the initial slumping phase and the subsequent flow produce very similar rates of overall entrainment. The rates of overall entrainment decrease with increasing aspect ratio, having values of 0.20, 0.16 and 0.14 lock volumes per lock length of propagation, for Experiments 1, 2 and 3, respectively. Although in Experiment 3 the rate of entrainment was smaller, a larger relative volume of ambient fluid was entrained in the early stages, because of the rapid mixing produced by the withdrawal of the gate.

The total rate of entrainment is a useful quantity, but does not indicate the extent of the mixing within the current. For example, a given quantity of ambient fluid entrained into the current either could be partially mixed with dense fluid to produce low concentration fluid, or could be more extensively mixed into the current to produce higher concentration fluid. To examine the extent of the mixing in each case it is necessary to consider the concentration distribution of the mixed fluid produced. In Fig. 4 we have chosen to consider six concentration bands. The difference in the ordinate values of any two isopleths gives the volume of fluid contained in the concentration band separating the isopleths. The divergence of the isolpeths indicates how the concentration distribution changes as the mixing progresses. It should be noted that the divergence of the isopleths is constrained by the condition that the total amount of salt in the flow is conserved, so that lower concentration bands may only grow at the expense of higher concentration bands.

In Experiment 1, the lower aspect ratio case of $R = 0.67$ (Fig. 4(a)), it can be seen that the low concentration isopleths exhibit stronger divergence. About half of the mixed fluid is of concentration between 0.05 and 0.40, and there is little mixed fluid of concentration between 0.40 and 0.80. This indicates that ambient fluid is not mixed extensively with current fluid in this case. This is consistent with the qualitative features of the mixing, owing to breaking interfacial waves confined to the region of the interface, described in Section 3.1. In Experiment 2, the case of $R = 1.00$ (Fig. 4(b)), there is stronger divergence of the lower concentration isopleths with most of the mixed fluid of concentration above 0.40. This indicates that ambient fluid is mixed more extensively within the current in this case, consistent with the qualitative features of the mixing within the strong vortex and deep wave breaking described in Section 3.1. In Experiment 3, the higher aspect ratio case of $R = 1.78$, the isopleths show more uniform divergence, indicating that ambient fluid is again being mixed more extensively into the current, but as ambient fluid is entrained into a region of previously mixed fluid, mixed fluid is produced more evenly across the concentration range. This concentration distribution is consistent with the qualitative features of the mixing, owing to wave overturning within a horizontal stratification, discussed in Section 3.1.

3.3. Front speed and head height

Despite these differences in internal structure, the non-dimensional velocities of propagation of the three currents were very similar, and constant over the common range of propagation of the three experiments. The total-depth based Froude

numbers defined by $\mathrm{Fr}_H \equiv (U_f/g'H)^{1/2}$, where U_f is the front speed, were 0.45, 0.45 and 0.46 for Experiments 1, 2 and 3, respectively, with an estimated error of ± 0.01. These values agree closely with the value of 0.46 obtained by Barr (1967) in an extensive series of experiments. The corresponding values of Reynolds number based on the front speed and half the total depth were 7000, 19 700 and 11 000, for the three experiments, respectively. In Experiment 3 the front speed remained constant for approximately eight lock lengths and then began to decelerate as $t^{-1/3}$, in accord with the similarity scaling.

The maximum head heights maintained by the three currents were also similar. The head is, however, an unsteady feature and it is difficult to be entirely consistent when measuring head height. The choice made here was to measure the maximum height h of the 0.05 iso-concentration contour within the head region. In each of the experiments the fractional height $\Phi \equiv h/H$ increased rapidly to somewhere between 0.45 and 0.55, and then began to gradually decrease.

It is interesting to note that the theoretical considerations of Benjamin (1968) for steady dissipationless currents predict Φ and Fr_H to be 0.5. It is difficult to compare the situation considered by Benjamin with the lock-release case because of the presence of mixing, the different upstream conditions, and the effects of the lower boundary layer, but the similarities in the values of Fr_H and Φ in the two situations are striking. Along with the insensitivity of these quantities to the differences in internal structure shown in the experiments, this may indicate that the dynamics determining the speed of propagation are a robust feature of the flow, and are not greatly affected by instability and mixing at the head.

4. Summary and conclusions

In this paper we have described a new experimental technique to determine the density structure of gravity currents. In the three experiments considered a common process by which gravity current fluid is mixed with ambient fluid can be identified. This is the detrainment of dense fluid from the head of the gravity current by breaking Kelvin–Helmholtz waves to produce stratified fluid in the rear of the current. The fluid detrained from the head is replaced by dense fluid from the rear and a sharp forward front is maintained. In this way, all of the fluid initially contained in the lock becomes mixed to some extent with the ambient fluid. As the current progresses further, the fluid detrained from the head is replaced by the densest (least mixed) fluid from the rear, and so, by a process of re-circulation through the head, the fluid of the gravity current becomes progressively diluted. In the later stages of the flow the developing region of stratification extends into the head of the gravity current.

As the experimental technique used here can only resolve across-stream averaged structure, we were not able to investigate directly the role played by three-dimensional structures in the mixing, particularly the importance of the 'lobes and clefts' at the nose of the current. These structures undoubtedly

contribute to the mixing, and further work will be required to understand their exact role.

The three experiments described in Section 3 also indicate that there is a broad range of internal structure associated with the initial development of lock-release gravity currents, and that differences in internal structure lead to different extents of mixing. These differences in internal structure and evolution can be attributed in part to changes in the aspect ratio of the lock, but other factors such as changes in Reynolds number and the relative importance of the disturbance caused by the withdrawal of the gate may also play a role. Work is currently in progress to investigate further the factors influencing the evolution of the flow and to quantify the mixing in more general terms. In particular, by considering longer time evolution, it will be possible to determine the extent to which gravity currents originating from different aspect ratio locks achieve self-similar behaviour at late times.

References

Barr, D.I.H., 1967. Densimetric exchange flow in rectangular channels. III: Large scale experiments. Houille-Blanche, 6(1967): 619–631.

Benjamin, T.B., 1968. Gravity currents and related phenomena. J. Fluid Mech., 31: 209–243.

Dalziel, S.B., 1993. Rayleigh–Taylor instability: experiments with image analysis. Dyn. Atmos. Oceans, 20: 127–153.

Hallworth, M.A., Phillips, J.C., Huppert, H.E. and Sparks, R.S.J., 1993. Entrainment in turbulent gravity currents. Nature, 362: 829–831.

Holford, J.M., 1994. The evolution of a front. Ph.D. Thesis. University of Cambridge.

Simpson, J.E., 1972. Effects of the lower boundary on the head of a gravity current. J. Fluid Mech., 53: 759–768.

Simpson, J.E., 1987. Gravity Currents in the Environment and in the Laboratory. Ellis Horwood, Chichester.

Simpson, J.E. and Britter, R.E., 1979. The dynamics of a gravity current advancing over a horizontal surface. J. Fluid Mech., 94: 447–495.